Materials Today Sustainability 26 (2024) 100753

Contents lists available at ScienceDirect

Materials Today Sustainability

journal homepage: www.journals.elsevier.com/materials-today-sustainability

Versatile cationic dual-layer hydrogel filtration system for sustainable solar steam generator

Casey Onggowarsito [a], Zeyu Shao [b], Shudi Mao [a], Stella Zhang [a], An Feng [a], Xiaowei Li [c], Edgar H.H. Wong [b,**], Qiang Fu [a,*]

[a] Centre for Technology in Water and Wastewater, School of Civil and Environmental Engineering, University of Technology Sydney, Ultimo, New South Wales, 2007, Australia
[b] Centre for Advanced Macromolecular Design (CAMD) and Australian Centre for NanoMedicine (ACN), School of Chemical Engineering, UNSW Australia, Sydney, NSW, 2052, Australia
[c] School of Environmental and Chemical Engineering, Shanghai University, Shanghai, 200444, China

ARTICLE INFO

Keywords:
Solar steam generation (SSG)
Dual layer hydrogel (DLH)
Desalination
Donnan repulsion affect
Cationic polymer
Antibacterial

ABSTRACT

Our increasing water demand has been an ongoing critical challenge due to water usages in areas such as industrial, agriculture, and domestic household. Conventional water production faces challenges, such as high investment, energy consumption, and brine discharge that may be unsustainable in the future. Solar steam generation (SSG) has been recently proposed by many researchers due to their sustainable and green water production method. Here we demonstrated the use of simple manufacturing and low-cost dual-layer hydrogel (DLH) system containing a double network of positive charged poly-[2-(acryloyloxy)ethyl] trimethyl ammonium chloride (PAETAC) and polyvinyl alcohol (PVA) bottom layer for fast water transport, as well as a broad light absorbing and heat generating PVA/graphene oxide (GO) top layer for fast water evaporation. As a result, the DLH was able to generate a high 3.12 kg m^{-2} h^{-1} water evaporation with 92% efficiency under 1 sun (kW m^{-2}) exposure. Furthermore, this DLH design allows for a safe and passive anti-salt and bacterial property due to PAETAC cationic chain, eliminating 99% salt and bacteria via Donnan repulsion and electrostatic interaction without the need of sunlight exposure.

1. Introduction

Water demand has been on a 1% per annum incline due to factors such as industrial, agriculture, and domestic water usage. Conventional water production systems such as thermal and membrane distillation are still our current solution towards countering the water demand. However, considering the high initial investment, high maintenance cost, and waste footprint that are caused by these systems may not be sustainable in the future [1,2]. Solar steam generation (SSG) is considered as an emerging technology to alleviate the water crisis due to its low-cost and clean water production. This is achieved through naturally heating photothermal materials (PTMs) absorbed water via sunlight for freshwater evaporation to occur [3]. Throughout many studies, the commonly used PTMs can be categorized into plasmonic metal nanoparticles, inorganic semiconductors, conjugated polymers, and carbon materials due to their high optical properties [4–6].

Despite this, there has been many challenges that occur throughout the development of SSG systems. One example of this is dealing with conductional and convectional heat loss between the SSG and bulk water [2,7,8]. As a result, most of the systems experienced an energy loss throughout the water evaporation process and therefore may reduce its evaporation efficiency [9–11]. Recent studies have suggested many insulative designs which can localized or isolate the heat generated for water evaporation [12,13]. One demonstrated insulating strategy can be seen in dual-layer systems. For example, Zhang et al. utilized a hydrophilic carbonized pulp foam material to reduce both conduction and convectional heat loss [14]. Besides carbonized hydrophilic insulators [15,16], PTM coating can also be used to produce dual-layer SSG [17,18]. An example of this can be seen in Meng et al. carbonized ZIF-8 PTM coating on top of a water absorbing and heat insulating wood sponge [19]. In addition, salt and bacterial filtration are another important factor to consider in freshwater production due to the major concerns

* Corresponding author.
** Corresponding author.
E-mail addresses: edgar.wong@unsw.edu.au (E.H.H. Wong), qiang.fu@uts.edu.au (Q. Fu).

https://doi.org/10.1016/j.mtsust.2024.100753
Received 16 January 2024; Accepted 16 March 2024
Available online 18 March 2024

that it could affect human health [2]. Salt filtration via SSG has been extensively discussed and have shown promising results of salt elimination in freshwater production [1,3,20]. However, there still lies a challenge in dealing with salt accumulation on a PTM surface. This could lead to a loss of light absorbing ability that can cause a reduction of evaporation efficiency [21]. Furthermore, bacterial filtration has been a challenge in conventional water treatment methods such as coagulation, flocculation, and chlorination. This is because of the existence of bacteria's viable but nonculturable (VBNC) state where some bacteria has the ability to be resuscitated while maintain its pathogenic nature when dormant [2]. Many SSG studies came to addressed this challenge via reactive oxygen species (ROS) or metallic nanoparticles ion. However, these approaches require active sunlight to disinfect bacteria activities. Additionally, the use of metallic nanoparticles may result in metallic ion leaching towards the bulk water which could result in detrimental health side effects [22–27].

To further address these challenges, we developed a novel dual-layer hydrogel (DLH) SSG system containing a positively charged bottom layer and a top light absorbing graphene oxide (GO) PTM layer with purpose of producing a future clean water production system. The combination of bottom layer allows for further heat insulation to avoid conductional/convectional heat loss towards the bulk water. In addition, the positively charged bottom layer also brings an affordable, passive, and safe approach to salt- and bacteria-filtration properties to the SSG due to the Donnan repulsion effect [28] as well as the strong zeta potential it possesses. As a result, this DLH system was able to generate an impressive 3.12 kg m^{-2} h^{-1} water evaporation with 90% efficiency under 1 sun simulation. In addition, the SSG demonstrated salt-resistant and filtration property with a stable 15-cycle, and exhibited a significant bacterial resistance towards the pathogen *Pseudomonas aeruginosa*.

2. Materials and methods

2.1. Materials

All reagents including polyvinyl alcohol (PVA, Mw: 89–98 kDa), [2-(acryloyloxy)ethyl]trimethyl ammonium chloride (AETAC, 80 wt% in H_2O), *N,N′*-methylenebis(acrylamide) (BIS, 99%), *N,N,N′,N′*-tetramethyl ethylenediamine (TEMED, 99% aqueous solution), ammonium persulfate (APS), glutaraldehyde (GA, 25% aqueous solution), graphene oxide (GO) were purchased from Sigma-Aldrich and used without further purification.

2.2. Synthesis of dual-layer hydrogel (DLH)

A semi-interpenetrating network comprising of PVA and PAETAC was synthesized as following: a specific amount of BIS powder was dissolved in 80 wt% AETAC solution to form different concentration PAETAC solutions. A certain amount of 10 wt% PVA solution was then added to each of these PAETAC solutions, followed by the addition of 75 μL of TEMED catalyst. These mixtures were polymerized by adding 1 mL of dissolved 100 mg APS initiator to form the bottom layer. For the top layer, 5 mL of 10 wt% PVA solution was thoroughly mixed with 5 mL of 1 mg/mL GO solution. Subsequently, 125 μL of 25 wt% GA was added to the PVA/GO mixture. These mixtures were quickly placed on top of each bottom layer network before it fully gelled. To catalyze the gelling process, 250 μL of 1 M HCl was added drop-wise onto the top layer. The obtained DLHs were then heated at 60 °C for 30 min. After heating, the DLHs were cooled to room temperature and frozen overnight, followed by freeze-drying them for 2 days.

2.3. Characterization

The frozen dried DLHs microstructure was captured by using Zeiss Supra 55VP scanning electron microscope (SEM).

Fourier-Transform infrared (FTIR) spectroscopy spectra of PVA, AETAC, GO, and DLHs were taken by SHIMADZU MIRacle 10 single reflection ATR accessory to demonstrate the hydrogels chemical content.

Absorption spectra of PVA, PVA/GO, and DLHs were recorded by Cary 7000 Universal Measurement ultraviolet–visible–near infrared (UV-VIS-NIR) spectrophotometer between the range of 200–2500 nm.

The vaporization enthalpies were studied using Q600 SDT Thermal Analyzer (DSC-TGA) and NETZSCH DSC 300 Caliris (DSC). Desalinated water collected from seawater evaporation was analyzed with Agilent 7900 ICP-MS.

2.4. Solar steam generation

Water evaporation experiments and freshwater collection were conducted using a laboratory solar light simulator (NBeT HSX-F3000 xenon light source) calibrated to 1 sun irradiation ($\leq$1 kW m^{-2}) under the setting of an inhouse built cabinet box. Solar light simulator was turned on approximately 20 min in advanced for the surrounding temperature to hit equilibrium before conducting water evaporation experiment. Water evaporation mass loss was measured by an analytical balance (OHAUS Pioneer IC-PX124) with a sequential recording of every 4 min. Hydrogel's surface temperature was captured and recorded using a thermal camera (Fluke PTi120) for every 5 min. Similarly, freshwater collection is done by evaporating a collected coastal seawater and highly concentrated (2x) seawater under the same circumstances. The vaporized freshwater was collected via a glass jar to be ICP.

2.5. Bacteria killing study

In order to evaluate the bactericidal efficiency of the hydrogel, a time-kill study was conducted against Gram-negative pathogen *Pseudomonas aeruginosa* ATCC 27853. Briefly, a single bacterial colony was cultured in 10 mL of Mueller-Hinton Broth (MHB) at 37 °C with 180 rpm shaking overnight. Subsequently, the overnight culture was diluted 1:10 in Phosphate-Buffered Saline (PBS) and 10 μL of the diluted bacterial solution was slowly dropped onto the surface of the hydrogel which was placed in a 6-well microplate (Costar, Corning). A negative control was also included wherein 10 μL of bacterial droplet was dropped into an empty well of the 6-well microplate. The plate was incubated for 1 h at 37 °C, before adding 2 mL of PBS into each sample well. The plate was then subjected to ultrasonication (150 W, 40 kHz) for 20 min to detach the bacteria from the surface. The viability of bacteria cells was determined by a drop plate method where the planktonic cells were serially diluted in PBS and plated onto Luria Bertani agar. After 24 h of incubation of 37 °C, bacteria colonies were counted and colony forming unit (CFU) analysis was performed. The assay included two replicates and were repeated in two independent experiments.

3. Results and discussion

The DLHs were synthesized using a 2-pot method, consisting of a semi-interpenetrating bottom layer and a top PTM layer (Scheme 1). The bottom layer was developed and tested with various mixture percentages of PVA and PAETAC (Supplementary Table 1). Notably, we first prepared a pristine PAETAC gel, however it was fragile due to its high swelling ratio. The introduction of high molecular weight PVA can significantly improve the mechanical robustness of the PAETAC network as well as the compatibility with the top layer. For the top PTM layer, a mixture of 10 wt% PVA and GO was thoroughly mixed and then carefully placed on top of the bottom layer, and gel formation was induced by adding crosslinker GA solution in the presence of HCl. Finally, the DLHs were heated at 60 °C for 30 m, followed by freeze-drying process. The chemical components of the resulting DLHs and control sample were listed in Table 1.

SEM analysis was conducted on both the top and bottom layers of the prepared DLHs to examine their microporous structure. As shown in

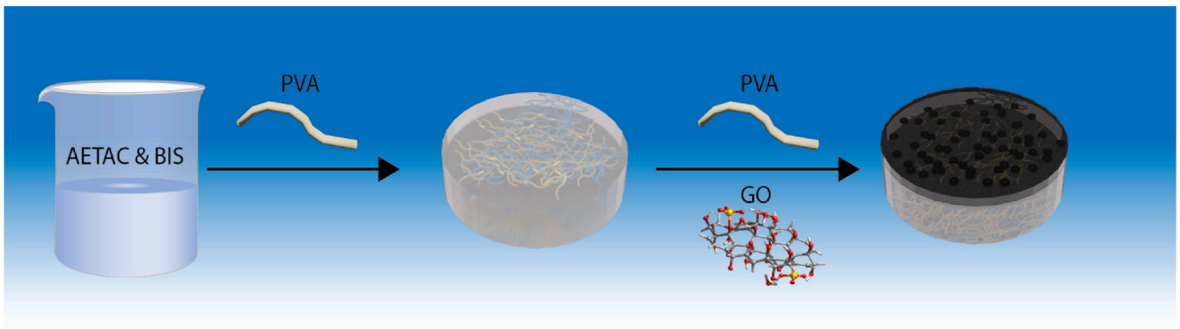

Scheme 1. Schematic illustration of the preparation of dual-layer hydrogel.

Table 1
Summary of the chemical components of the DLHs.

Entry	Bottle layer (wt%)	Top layer (wt %)	Vaporization enthalpy (J g^{-1})
DLH1	3%PVA/5%PAETAC	10%PVA/GO	1602
DLH2	3%PVA/10%PAETAC		1650
DLH3	10%PVA/5%PAETAC		1443
DLH4	10%PVA/10% PAETAC		1532
H5	n/a		2094

Fig. 1a and b, both DLHs cross-sectional top and bottom layers exhibited numerous porous microchannels, facilitating a rapid water absorption and evaporation rate via capillary effect [29]. Moreover, the bottom layer also displayed significant surface roughness highlighted in Fig. 1c, contributing to increased hydrophilicity and improved water absorption capacity. Furthermore, DLHs hydrogel black top layer has a high surface roughness (Fig. 1d), which enhances light absorption, resulting in good photothermal performance.

In addition to the hydrogel porous microchannels, hydrophilic groups contained within the polymer matrix such as hydroxyl groups from PVA, ammonium groups from PAETAC, and carboxyl groups from GO are a major contributor in increasing water absorption/transport capability [3,30–32]. The presence of hydrophilic groups can be observed in Fig. 2a, where the O–H stretching at 3292 cm^{-1} indicates the presence of the PVA hydroxyl group in both top and bottom layers. Additionally, the 3029 cm^{-1} peak in bottom layer (PVA/PAETAC) can be attributed to the N–H stretching of ammonium of PAETAC [3,30,31]. In addition, the observation of C═O stretching at 1732 cm^{-1} indicates the presence of PAETAC in the bottom layer [30,31,33]. Moreover, the C–H bend at 1433 cm^{-1} reveals the presence of PVA/PAETAC alkane vibrations [30,31]. Lastly, the C–O stretching at 1088 cm^{-1} can be observed in both top and bottom layers, indicating the characteristic presence of PVA [3,34,35]. The UV-VIS-NIR spectra in Fig. 2b provides compelling evidence of the broad light absorption capability of the top layer of DLHs. As seen, the PVA/GO top layer exhibits extensive light absorption across the UV to IR region, efficiently harnessing a significant amount of light energy and converting it into heat [2]. In contrast, the PVA/PAETAC bottom layer demonstrates low light absorption and primarily near the FIR range. This distinction in light absorption is noteworthy as it directly impacts the temperature generated by the top layer under steady state. Specifically, the top surface reaches high

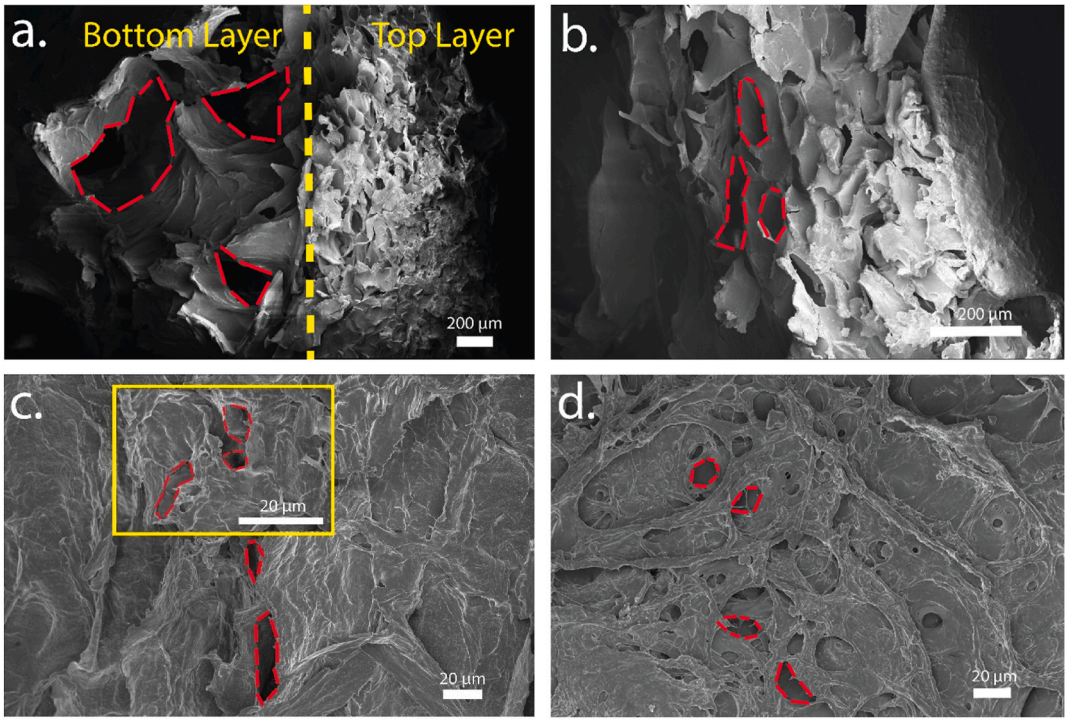

Fig. 1. (a) Cross-sectional microporous structure of both DLH bottom and (b) top layer. (c) Bottom and (d) top surface structure containing surface roughness and microporous structure for water and vapor transfer.

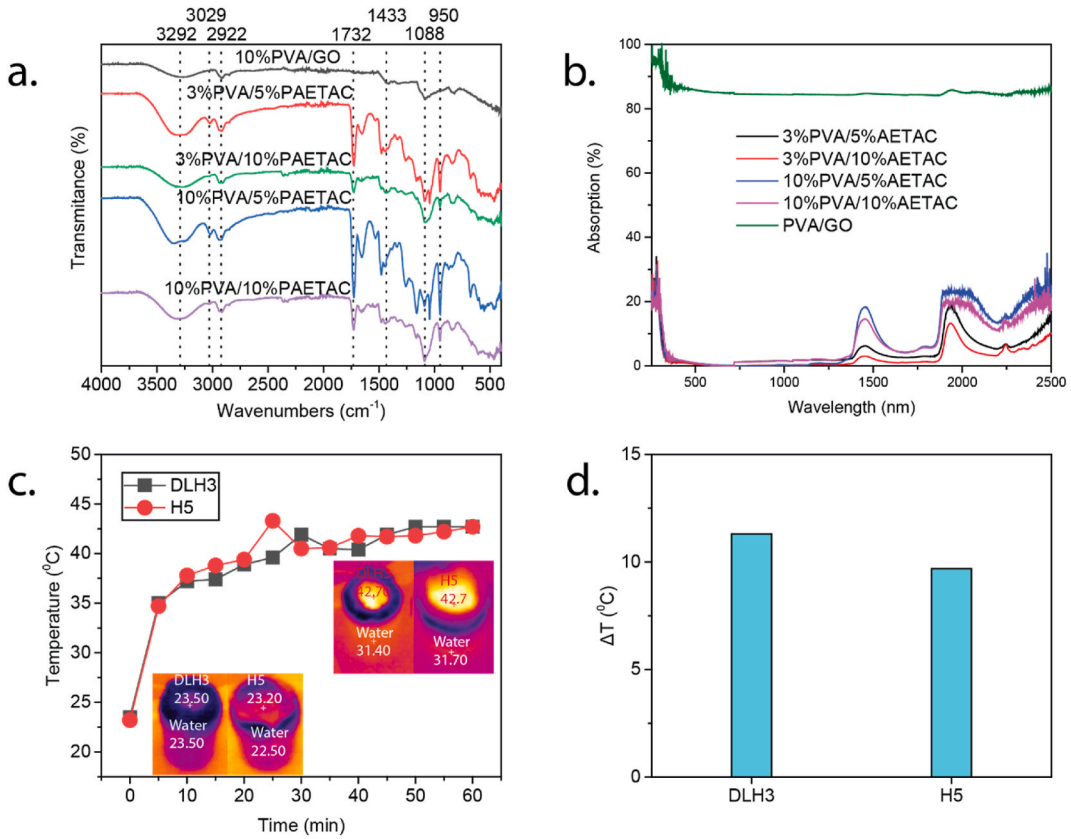

Fig. 2. (a) FTIR and (b) UV spectra of top and bottom layer of DLH hydrogels. (c) DLH3 and H5 surface temperature generated and (d) average temperature difference between surface temperature with the surrounding bulk water throughout 1 h water evaporation under 1 sun.

temperatures relatively quickly, achieving a qualitative increase in temperature within approximately 10 min. The maximum temperature observed an average of approximately 40 °C as shown in Fig. 2c. Besides generating an impressive thermal surface temperature, DLH3 also contain a dual-layer heat management insulation to reduce the amount of heat loss towards the bulk water as demonstrated by the temperature difference between surface and bulk water shown in Fig. 2d.

In this study, we tune the concentrations of PVA and PAETAC, and obtained DLH with variable vaporization enthalpy as shown in Table 1 and Fig. 3a. The DSC results (Supplementary Fig. 1) demonstrated all DLHs and H5 contain lower vaporization enthalpy compared to pure water due to PVA, PAETAC, and GO hydrophilic groups as shown by the FTIR results previously. The hydrophilic groups contained in both DLHs and H5 leads to the intermediate water content presence in the gel matrix as shown by the Raman spectra in Supplementary Fig. 3. This therefore allows for water evaporation in the form of small clusters of water molecules, lowering the vaporization enthalpy as less energy is needed to break the water molecule bonds [2,36,37]. As demonstrated in Fig. 3b, when we increased the concentration of PAETAC, the obtained DLH displayed enhanced water absorption capability (*aka.* swelling ratio). In addition, the half-swollen time which signifies the water transport rate throughout water evaporation process reduces as PAETAC concentration increases. This may be the result of DLH oversaturation as PAETAC absorbs water too rapidly, resulting in higher free water content and vaporization enthalpy due to the limited intermediate water content. Despite this, the results indicate the promising potential of these hydrogels in water retention and release applications. Interestingly, we observed that the DLH3 with 10%PVA/5%PAETAC bottom layer content appeared to strike an optimal concentration balance between a low vaporization enthalpy and efficient water absorption rate.

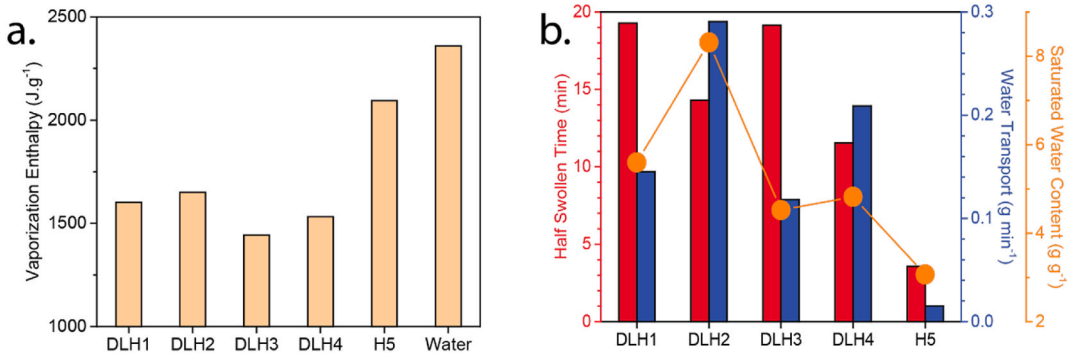

Fig. 3. (a) Comparison of DLHs, H5, and theoretical bulk water vaporization enthalpy at 100 °C. (b) Tuneable water absorption capability of DLHs compared with H5 absorption characteristic.

As shown by Fig. 4a, all water evaporation performances were obtained through solar steam generation (SSG) experiment. This procedure involves recording the water mass loss caused by the light exposure under constant illumination of 1 sun (1 kW m^{-2}). The solar light simulator was turned on 20 min prior to conducting SSG. To prevent any excess bulk water evaporation, polystyrene foam was strategically placed to cover the exposed water surface area during ongoing SSG for both H5 and DLH hydrogels. As demonstrated in Fig. 4b and c, the H5 and DLH hydrogels were able to demonstrate a significant increase in water evaporation compared to the control consisting of just pure water. This is mainly due to their low vaporization enthalpy as discussed previously, allowing for easy water evaporation. Moreover, DLH hydrogels water evaporation rate as shown in Fig. 4c showed a similar trend towards its vaporization enthalpy and water absorption capability shown in Fig. 3a and b, demonstrating the correlation between these three factors. Noticeably, DLH 3 generated the highest water evaporation rate of 3.12 kg m^{-2} h^{-1} with an impressive 92% solar to thermal conversion efficiency. As shown in Supplementary Equation 3, DLH3 high conversion efficiency is due to its previously discussed high thermal generation management, as well as its optimal balance between low vaporization enthalpy and fast water absorption rate contributes to its high conversion efficiency as discussed previously. Moreover, DLH3 water evaporation performance was significantly higher than other recent dual-layer hydrogels performance as shown in Fig. 4d.

Desalination and stability testing was conducted using both standard and double (2x) concentrations of local coastal seawater from Sydney. In the experimental setup as shown in Fig. 5a, the DLH3 hydrogel was configured similarly to the SSG experiment as described earlier. DLH3 hydrogel was subjected to 1 sun exposure and contained within a glass container to capture desalinated vapors for 1-h cycle. Remarkably, DLH3 consistently achieved desalination of normal seawater concentration, exhibiting a rate of 2.17 kg m^{-2} h^{-1} over 15 desalination cycles, as shown in Fig. 5b. After each cycle, DLH3 was cooled down to room temperature. Furthermore, no salt accumulation was observed throughout the desalination cycles. This impressive salt rejection capability of DLH3 can be attributed to the Donnan repulsion affect potentially induced by the PAETAC cationic groups [2]. This salt rejection property allows DLH3 to filter over 99% salts (Na^+, Mg^{2+}, K^+, and Ca^{2+}), thereby generating freshwater that surpasses the WHO drinking water standard [38].

DLH3 antibacterial study was carried out using the Gram-negative pathogenic bacterium *Pseudomonas aeruginosa*, commonly found in agricultural soil, and known for its potential cause of range of lung diseases [39,40]. Upon exposure to this pathogen, DLH3 was subjected to a 1-h incubation at 37 °C. The results were striking, showcasing DLH3's robust antibacterial property, eliminating over 99% of the pathogenic bacteria, as quantified by the CFU count in Fig. 5e. This remarkable antibacterial performance is also attributed to the PAETAC cationic groups. The PAETAC positively charged chains can induce electrostatic interactions with gram-negative bacterial membranes, facilitating membrane penetration and subsequently triggering bacterial death [41–45]. This innovative antibacterial approach offers the distinct advantage of passive bacterial filtration around the clock, independent of external factors such as sunlight or UV exposure, setting it apart from conventional SSG systems [22,23]. Furthermore, DLH3's synthesis process maintains a cost-effective edge over other systems that rely on intricate nanoparticles for antibacterial effectiveness. Additionally, DLH3 is a safer alternative as it avoids metal ions contamination released by the metallic nanoparticles used for antibacterial mechanism [24–27].

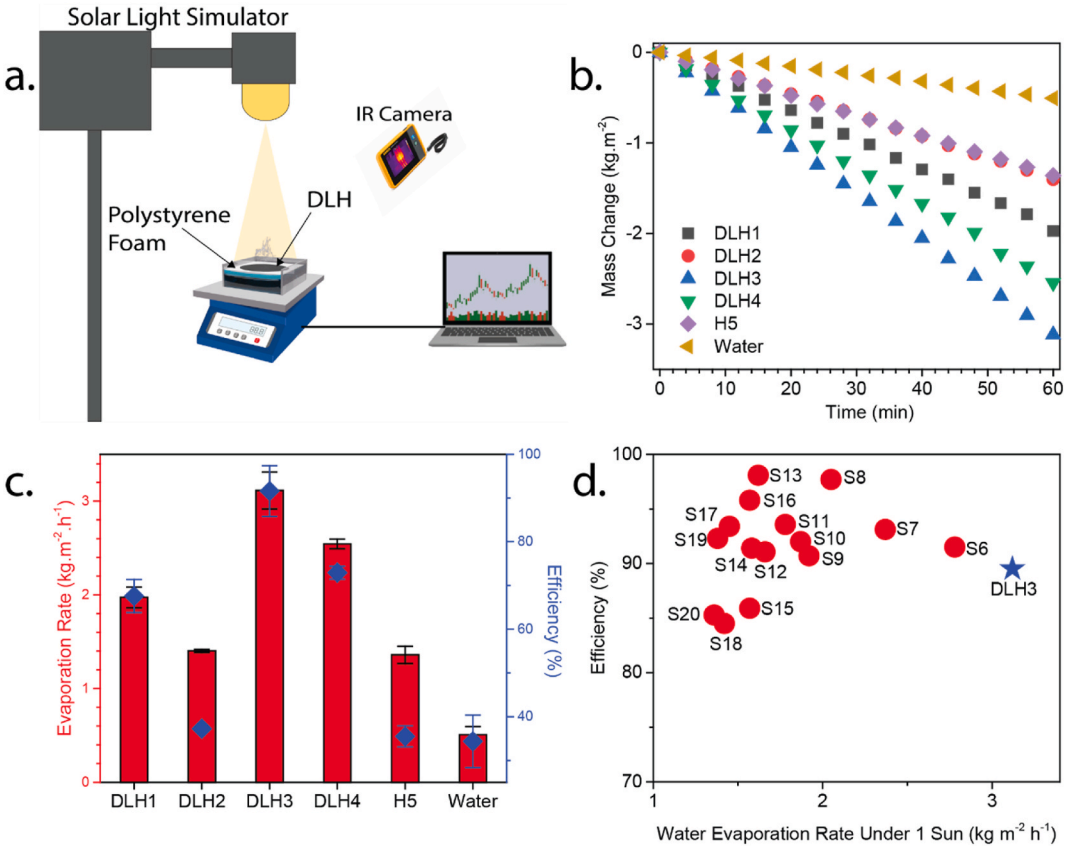

Fig. 4. (a) Schematic diagram of SSG experiment. (b) Water mass loss, (c) water evaporation rate and solar to thermal conversion efficiency of DLH hydrogels, H5 hydrogel, and pure water. (d) Other dual-layer hydrogels water evaporation and efficiency performance in comparison to DLH3 in this study.

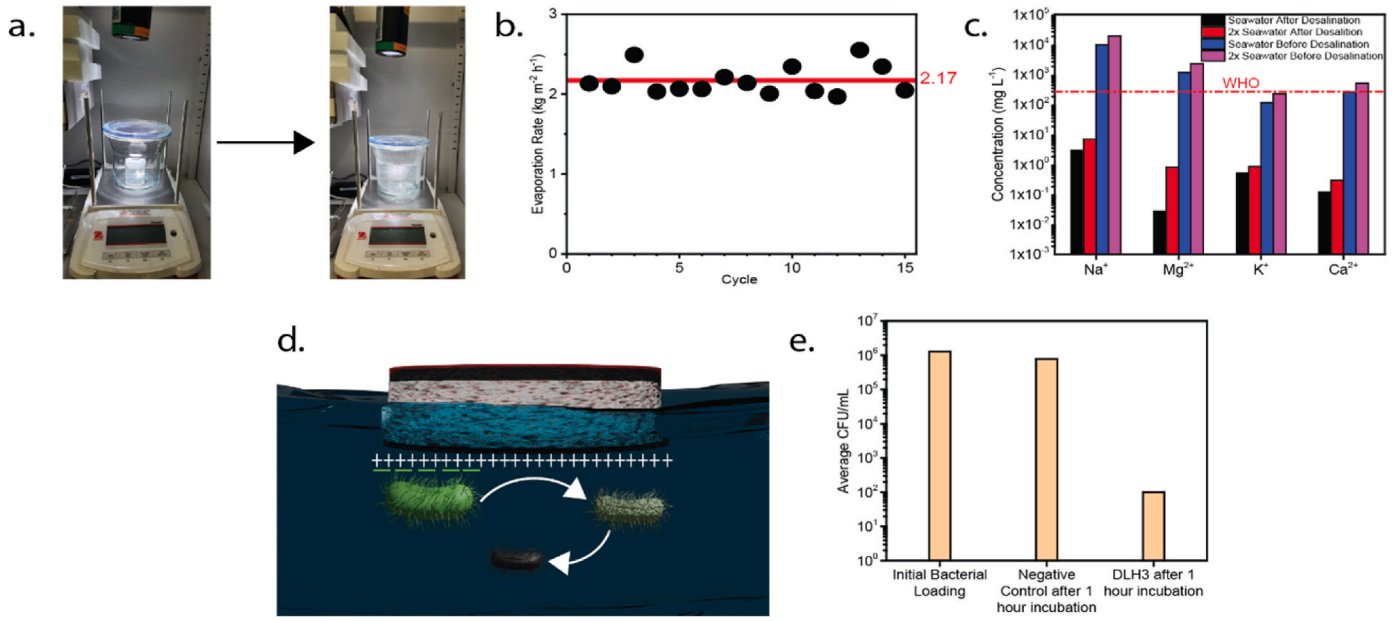

Fig. 5. (a) Before and after desalination testing. (b) DLH3 desalination stability result after 15 cycles of evaporation. (c) ICP-MS results of DLH3 desalinated seawater salt ions concentration. (d) Schematic diagram of DLH antibacterial mechanism. (e) CFU bacterial colony count of DLH3 after being exposed with Gram-negative pathogenic *Pseudomonas aeruginosa* with 1 h incubation period.

4. Conclusion

In pursuit of a versatile water filtration application, a groundbreaking DLH hydrogel was meticulously designed. This is achieved by the combination of upper layer heat generation management containing broad light absorption PTM, insulated by a fast water absorption bottom layer. The balance between having both robust mechanical structure of these layers and water absorption capability was strategically achieved through the PVA encapsulation of both GO PTM and high water-absorbing PAETAC. The optimized DLH3 was able to outperform other dual-layer SSG systems with an impressive water evaporation rate of 3.12 kg m^{-2} h^{-1} with an efficiency of 92% solar to thermal conversion due to its high thermal generation management, low vaporization enthalpy, and fast water absorption. Moreover, DLH3 was able to demonstrate its primary purpose of versatile water filtration application due to its salt resistant and outstanding antibacterial property caused by the positively charged PAETAC bottom layer.

CRediT authorship contribution statement

Casey Onggowarsito: Investigation, Methodology, Writing – original draft. **Zeyu Shao:** Investigation. **Shudi Mao:** Investigation, Writing – review & editing. **Stella Zhang:** Investigation, Writing – review & editing. **An Feng:** Investigation. **Xiaowei Li:** Investigation, Validation. **Edgar H.H. Wong:** Investigation, Supervision. **Qiang Fu:** Writing – review & editing, Funding acquisition, Resources, Supervision.

Declaration of competing interest

The authors declare that they have no known competing financial interests or personal relationships that could have appeared to influence the work reported in this paper.

Data availability

Data will be made available on request.

Acknowledgements

Q. F. acknowledges the Australian Research Council under the Future Fellowship (FT180100312). C. O. acknowledges support of the Australian Government Research Training Program Scholarship from the University of Technology Sydney.

Appendix A. Supplementary data

Supplementary data to this article can be found online at https://doi.org/10.1016/j.mtsust.2024.100753.

References

[1] S. Mao, M.A.H. Johir, C. Onggowarsito, A. Feng, L.D. Nghiem, Q. Fu, Recent developments of hydrogel based solar water purification technology, Mater. Adv. 3 (3) (2022) 1322–1340, https://doi.org/10.1039/D1MA00894C.
[2] C. Onggowarsito, A. Feng, S. Mao, L.N. Nguyen, J. Xu, Q. Fu, Water harvesting strategies through solar steam generator systems, ChemSusChem 15 (23) (2002) e202201543, https://doi.org/10.1002/cssc.202201543.
[3] C. Onggowarsito, A. Feng, S. Mao, S. Zhang, I. Ibrahim, L. Tijing, Q. Fu, H.H. Ngo, Development of an innovative MnO2 nanorod for efficient solar vapor generator, Env, Met. Funct. Mater. 1 (2) (2022) 196–203, https://doi.org/10.1016/j.efmat.2022.08.001.
[4] X. Wu, G.Y. Chen, G. Owens, D. Chu, H. Xu, Photothermal materials: a key platform enabling highly efficient water evaporation driven by solar energy, Mater. Today Energy 12 (2019) 277–296, https://doi.org/10.1016/j.mtener.2019.02.001.
[5] P. Wang, Emerging investigator series: the rise of nano-enabled photothermal materials for water evaporation and clean water production by sunlight, Environ. Sci.: Nano 5 (5) (2018) 1078–1089, https://doi.org/10.1039/C8EN00156A.
[6] W. Guan, Y. Guo, G. Yu, Carbon materials for solar water evaporation and desalination, Small 17 (48) (2021) 2007176, https://doi.org/10.1002/smll.202007176.
[7] T.A. Cooper, S.H. Zandavi, G.W. Ni, Y. Tsurimaki, Y. Huang, S.V. Boriskina, G. Chen, Contactless steam generation and superheating under one sun illumination, Nat. Commun. 9 (1) (2018) 5086, https://doi.org/10.1038/s41467-018-07494-2.
[8] X. Song, H. Song, S. Wang, J. Liu, L. Zhou, J. Xu, K. Chen, Enhancement of solar vapor generation by a 3D hierarchical heat trapping structure, J. Mater. Chem. A 7 (46) (2019) 26496–26503, https://doi.org/10.1039/C9TA09554C.
[9] W. Zhang, Z. Li, C. Zhang, Y. Lin, H. Zhu, Z. Meng, D. Wu, Improvement of the efficiency of volumetric solar steam generation by enhanced solar harvesting and energy management, Renew. Energy 183 (2022) 820–829, https://doi.org/10.1016/j.renene.2021.11.054.
[10] H.D. Kiriarachchi, A.A. Hassan, F.S. Awad, M.S. El-Shall, Metal-free functionalized carbonized cotton for efficient solar steam generation and wastewater treatment, RSC Adv. 12 (2) (2022) 1043–1050, https://doi.org/10.1039/D1RA08438K.

[11] M.M. Ghafurian, H. Niazmand, E. Ebrahimnia-Bajestan, H. Elhami Nik, Localized solar heating via graphene oxide nanofluid for direct steam generation, J. Therm. Anal. Calorim. 135 (2) (2019) 1443–1449, https://doi.org/10.1007/s10973-018-7496-0.
[12] B. Soo Joo, I. Soo Kim, I. Ki Han, H. Ko, J. Gu Kang, G. Kang, Plasmonic silicon nanowires for enhanced heat localization and interfacial solar steam generation, Appl. Surf. Sci. 583 (2022) 152563, https://doi.org/10.1016/j.apsusc.2022.152563.
[13] B. Yu, Y. Wang, Y. Zhang, Z. Zhang, Nanoporous black silver film with high porosity for efficient solar steam generation, Nano Res. 16 (4) (2023) 5610–5618, https://doi.org/10.1007/s12274-022-5068-x.
[14] Y. Zhang, W. Deng, M. Wu, Z. Liu, G. Yu, Q. Cui, C. Liu, P. Fatehi, B. Li, Robust, scalable, and cost-effective surface carbonized pulp foam for highly efficient solar steam generation, ACS Appl. Mater. Interfaces 15 (5) (2023) 7414–7426, https://doi.org/10.1021/acsami.2c21260.
[15] C. Wang, Y. Wang, M. Yan, W. Zhang, P. Wang, W. Guan, S. Zhang, L. Yu, J. Feng, Z. Gan, L. Dong, Highly efficient self-floating jellyfish-like solar steam generators based on the partially carbonized Enteromorpha aerogel, J. Colloid Interface Sci. 630 (2023) 297–305, https://doi.org/10.1016/j.jcis.2022.09.133.
[16] X. Hou, H. Sun, F. Dong, H. Wang, Z. Bian, 3D carbonized grooved straw with efficient evaporation and salt resistance for solar steam generation, Chemosphere 315 (2023) 137732, https://doi.org/10.1016/j.chemosphere.2022.137732.
[17] S. Ge-Zhang, H. Yang, H. Mu, Interfacial solar steam generator by MWCNTs/carbon black nanoparticles coated wood, Alex. Eng. J. 63 (2023) 1–10, https://doi.org/10.1016/j.aej.2022.08.002.
[18] R. Mehrkhah, K. Goharshadi, E.K. Goharshadi, H.-S. Sajjadizadeh, Multifunctional photoabsorber for highly efficient interfacial solar steam generation and wastewater treatment, ChemistrySelect 8 (6) (2023) e202204386, https://doi.org/10.1002/slct.202204386.
[19] T. Meng, Z. Li, Z. Wan, J. Zhang, L. Wang, K. Shi, X. Bu, S.M. Alshehri, Y. Bando, Y. Yamauchi, D. Li, X. Xu, MOF-Derived nanoarchitectured carbons in wood sponge enable solar-driven pumping for high-efficiency soil water extraction, Chem. Eng. J. 452 (2023) 139193, https://doi.org/10.1016/j.cej.2022.139193.
[20] F. Zhao, X. Zhou, Y. Shi, X. Qian, M. Alexander, X. Zhao, S. Mendez, R. Yang, L. Qu, G. Yu, Highly efficient solar vapour generation via hierarchically nanostructured gels, Nat. Nanotechnol. 13 (6) (2018) 489–495, https://doi.org/10.1038/s41565-018-0097-z.
[21] M. Sheng, Y. Yang, X. Bin, S. Zhao, C. Pan, F. Nawaz, W. Que, Recent advanced self-propelling salt-blocking technologies for passive solar-driven interfacial evaporation desalination systems, Nano Energy (2021) 106468, https://doi.org/10.1016/j.nanoen.2021.106468.
[22] J. Wang, Z. Chen, L. Feng, F. Yu, C. Ran, N. Xu, Z. Jia, C. Li, Y. Zheng, W. Shi, M. Li, Plants transpiration-inspired antibacterial evaporator with multiscale structure and low vaporization enthalpy for solar steam generation, Nano Energy 114 (2023) 108631, https://doi.org/10.1016/j.nanoen.2023.108631.
[23] M.S. Irshad, N. Arshad, G. Liu, N. Mushtaq, A.A. Lashari, W. Qin, M.S. Asghar, H. Li, X. Wang, Biomass-printed hybrid solar evaporator derived from bio-polluted invasive species, a potential step toward carbon neutrality, ACS Appl. Mater. Interfaces 15 (13) (2023) 16607–16620, https://doi.org/10.1021/acsami.2c20207.
[24] C. Gao, Y. Chen, Q. Wang, B. Zhou, J. Li, J. Mao, J. Guo, Multifunctional fabrics embedded with polypyrrole-silver/silver chloride nanocomposites for solar-driven steam generation and photocatalytic decontamination, Sep. Purif. Technol. 323 (2023) 124477, https://doi.org/10.1016/j.seppur.2023.124477.
[25] O.R. Hayes, A.A. Ibrahim, M.S. Adly, S.E. Samra, A.M.A. Ouf, S.A. El-Hakam, A. I. Ahmed, Solar-driven seawater desalination via plasmonic hybrid MOF/polymer and its antibacterial activity, RSC Adv. 13 (27) (2023) 18525–18537, https://doi.org/10.1039/D3RA02242K.
[26] A. Allahbakhsh, Z. Jarrahi, G. Farzi, A. Shavandi, Solar-powered and antibacterial water purification via Cu-BTC-embedded reduced graphene oxide nanocomposite aerogels, Chem. Eng. J. 467 (2023) 143472, https://doi.org/10.1016/j.cej.2023.143472.
[27] X. Fan, Y. Peng, Y. Li, Y. Yang, Z. You, Y. Xu, Oriented porous hydrogel with excellent anti-salt and antibacterial properties for high-performance interfacial solar steam generation, J. Environ. Chem. Eng. 11 (5) (2023) 110668, https://doi.org/10.1016/j.jece.2023.110668.
[28] Q. Xiao, Y. Zhu, Y. Xi, X. Kong, X. Ye, Z. Zhang, C. Qiu, W. Xu, S. Cheng, J. Zhang, M. Jia, E. Sun, H. Lin, J. Wang, Highly charged hydrogel with enhanced donnan exclusion toward ammonium for efficient solar-driven water remediation, Chem. Eng. J. 430 (2022) 133019, https://doi.org/10.1016/j.cej.2021.133019.
[29] Y. Yang, Y. He, S. Yang, D. Dong, J. Zhang, J. Ding, J. Zhang, Y.M. Chen, Tough, durable and saline-tolerant CNT@Gel-nacre nanocomposite for interfacial solar steam generation, J. Colloid Interface Sci. 650 (2023) 182–192, https://doi.org/10.1016/j.jcis.2023.06.148.
[30] A. Onder, P. Ilgin, H. Ozay, O. Ozay, Removal of dye from aqueous medium with pH-sensitive poly[(2-(acryloyloxy)ethyl]trimethylammonium chloride-co-1-vinyl-2-pyrrolidone] cationic hydrogel, J. Environ. Chem. Eng. 8 (5) (2020) 104436, https://doi.org/10.1016/j.jece.2020.104436.
[31] S.I. Qashou, E.F.M. El-Zaidia, A.A.A. Darwish, T.A. Hanafy, Methylsilicon phthalocyanine hydroxide doped PVA films for optoelectronic applications: FTIR spectroscopy, electrical conductivity, linear and nonlinear optical studies, Phys. B Condens. Matter 571 (2019) 93–100, https://doi.org/10.1016/j.physb.2019.06.063.
[32] Q.-C. Tan, X.-S. Jiang, L. Chen, J.-F. Huang, Q.-X. Zhou, J. Wang, Y. Zhao, B. Zhang, Y.-N. Sun, M. Wei, X. Zhao, Z. Yang, W. Lei, Y.-F. Tang, Z.-X. Wu, Bioactive graphene oxide-functionalized self-expandable hydrophilic and osteogenic nanocomposite for orthopaedic applications, Mater. Today Bio 18 (2023) 100500, https://doi.org/10.1016/j.mtbio.2022.100500.
[33] F. Ozsoy, B. Ozdilek, A. Onder, P. Ilgin, H. Ozay, O. Ozay, Graphene nanoplate incorporated Gelatin/poly(2-(Acryloyloxy)ethyl trimethylammonium chloride) composites hydrogel for highly effective removal of Alizarin Red S from aqueous solution, J. Polym. Res. 29 (11) (2022) 481, https://doi.org/10.1007/s10965-022-03327-5.
[34] S. Durmuş, B. Yilmaz, M.R. Kıvanç, A. Onder, P. Ilgin, H. Ozay, O. Ozay, Synthesis, characterization, and in vitro drug release properties of AuNPs/p(AETAC-co-VI)/Q nanocomposite hydrogels, Gold Bull. 54 (2) (2021) 75–87, https://doi.org/10.1007/s13404-021-00295-4.
[35] A. Onder, M.R. Kıvanç, P. Ilgin, H. Ozay, O. Ozay, Synthesis of p(HEMA-co-AETAC) nanocomposite hydrogel with vinyl-function montmorillonite nanoparticles and effective removal of methyl orange from aqueous solution, J. Macromol. Sci. 60 (2) (2023) 108–123, https://doi.org/10.1080/10601325.2023.2169155.
[36] L. Zang, L. Sun, S. Zhang, C. Finnerty, A. Kim, J. Ma, B. Mi, Nanofibrous hydrogel-reduced graphene oxide membranes for effective solar-driven interfacial evaporation and desalination, Chem. Eng. J. 422 (2021) 129998, https://doi.org/10.1016/j.cej.2021.129998.
[37] B. Yang, Z. Zhang, P. Liu, X. Fu, J. Wang, Y. Cao, R. Tang, X. Du, W. Chen, S. Li, H. Yan, Z. Li, X. Zhao, G. Qin, X.-Q. Chen, L. Zuo, Flatband λ-Ti3O5 towards extraordinary solar steam generation, Nature (2023), https://doi.org/10.1038/s41586-023-06509-3.
[38] L. Zuo, Y. Li, L. Cheng, T. Yu, Y. Che, S. Yan, K.V. Yurievich, T. Bian, D. Chen, Polydopamine modified ZIF-L/sodium alginate composites as the highly efficient photothermal membrane for solar steam generation, Sep. Purif. Technol. 308 (2023) 122859, https://doi.org/10.1016/j.seppur.2022.122859.
[39] S. Grandy, M. Scur, K. Dolan, R. Nickerson, Z. Cheng, Using model systems to unravel host–Pseudomonas aeruginosa interactions, Environ. Microbiol. 25 (10) (2023), https://doi.org/10.1111/1462-2920.16440.
[40] N. Reyne, A. McCarron, P. Cmielewski, D. Parsons, M. Donnelley, To bead or not to bead: a review of Pseudomonas aeruginosa lung infection models for cystic fibrosis, Front. Physiol. 14 (2023), https://doi.org/10.3389/fphys.2023.1104856.
[41] X. Du, M. Ma, Y. Zhang, X. Yu, L. Chen, H. Zhang, Z. Meng, X. Jia, J. Chen, Q. Meng, C. Li, Synthesis of cationic biphen[4, 5]arenes as biofilm disruptors, Angew. Chem. 135 (21) (2023), https://doi.org/10.1002/ange.202301857.
[42] Y. Wu, Q. He, X. Che, F. Liu, J. Lu, X. Kong, Effect of number of lysine motifs on the bactericidal and hemolytic activity of short cationic antimicrobial peptides, Biochem. Biophys. Res. Commun. 648 (2023) 66–71, https://doi.org/10.1016/j.bbrc.2023.01.094.
[43] H. Wang, Z. Chen, S. Cheng, R. Li, X. Pan, C. Zhang, H. Gu, A. Xie, W. Dong, Synthesis of cationic hydrogels with tunable physicochemical properties for antibacterial applications, Eur. Polym. J. 173 (2022) 111228, https://doi.org/10.1016/j.eurpolymj.2022.111228.
[44] E. Wulandari, R. Namivandi-Zangeneh, P.R. Judzewitsch, R. Budhisatria, A. H. Soeriyadi, C. Boyer, E.H.H. Wong, Silk sponges with surface antimicrobial activity, ACS Appl. Bio Mater. 4 (1) (2021) 692–700, https://doi.org/10.1021/acsabm.0c01222.
[45] E. Wulandari, R. Budhisatria, A.H. Soeriyadi, M. Willcox, C. Boyer, E.H.H. Wong, Releasable antimicrobial polymer-silk coatings for combating multidrug-resistant bacteria, Polym. Chem. 12 (48) (2021) 7038–7047, https://doi.org/10.1039/D1PY01219C.